Title	Endomicroscopic optical coherence tomography for cellular resolution imaging of gastrointestinal tracts
Author(s)	Luo, Yuemei; Cui, Dongyao; Yu, Xiaojun; Bo, En; Wang, Xianghong; Wang, Nanshuo; Braganza, Cilwyn S.; Chen, Shufen; Liu, Xinyu; Xiong, Qiaozhou; Chen, Si; Chen, Shi; Liu, Linbo
Citation	Luo, Y., Cui, D., Yu, X., Bo, E., Wang, X., Wang, N., et al. (2018). Endomicroscopic optical coherence tomography for cellular resolution imaging of gastrointestinal tracts. Journal of Biophotonics, in press.
Date	2017
URL	http://hdl.handle.net/10220/44292
Rights	

Article type: Full Article

Endomicroscopic optical coherence tomography for cellular resolution imaging of gastrointestinal tracts

Yuemei Luo[1], Dongyao Cui[1], Xiaojun Yu[1], En Bo[1], Xianghong Wang[1], Nanshuo Wang[1], Cilwyn Shalitha Braganza[1], Shufen Chen[1], Xinyu Liu[1], Qiaozhou Xiong[1], Si Chen[1], Shi Chen[1], and Linbo Liu[1,2,]*

*Corresponding Author: E-mail: liulinbo@ntu.edu.sg

[1]50 Nanyang Ave, School of Electrical and Electronic Engineering, Nanyang Technological University, 639798, Singapore
[2]62 Nanyang Dr, School of Chemical and Biomedical Engineering, Nanyang Technological University, 637459, Singapore

Keywords: Optical coherence tomography, Endoscopic imaging, Fiber optics Imaging, Medical and biological imaging, Gastrointestinal tracts

Short title: Y. Luo, et al.: Endomicroscopic OCT for cellular resolution imaging of GI tracts

Our ability to detect neoplastic changes in gastrointestinal (GI) tracts is limited by the lack of an endomicroscopic imaging tool that provides cellular-level structural details of GI mucosa over a large tissue area. In this paper, we report a fiber-optic based micro-optical coherence tomography (μOCT) system and demonstrate its capability to acquire cellular-level details of GI tissue through circumferential scanning. The system achieves an axial resolution of 2.48 μm in air and a transverse resolution of 4.8 μm with a depth-of-focus (DOF) of ~150 μm. To mitigate the issue of limited DOF, we used a rigid sheath to maintain a circular lumen and center the distal end optics. The sensitivity is tested to be 98.8 dB with an illumination power of 15.6 mW on the sample. With fresh swine colon tissues imaged *ex vivo*, detailed structures such as crypt lumens and goblet cells can be clearly resolved, demonstrating that this fiber-optic μOCT system is capable of visualizing cellular-level morphological features. We also demonstrate that time-lapsed frame averaging and imaging speckle reduction are essential for clearly visualizing cellular level details. Further development of a clinically viable μOCT endomicroscope is likely to improve the diagnostic outcome of GI cancers.

1. Introduction

Intestinal crypts, usally found as the invaginations, are the home for vigorous proliferation of epithelial cell, and thus are vital to fuel the self-renewal process of the epithelium [1]. Goblet cells are the glandular epithelium cells to produce gel-like mucin to maintain the homeostasis [2, 3]. The intestinal crypts together with the goblet cells are key architectures residing throughout the large intestine, and are also critical indicators of pre-malignant lesion for early detection of intestinal cancers [4]. Particularly, in the colon, the structural alterations of crypts and goblet cells are associated with the assessment of ulcerative colitis and even colonic cancers [5, 6]. Therefore, the visualization of intestinal crypts and the goblet cells is of great importance to detect early lesions of gastrointestinal (GI) tracts.

Among current screening and surveillance tools, white light endoscopy (WLE), followed by random excisional biopsy is the gold standard to investigate intraepithelial neoplasia in GI tracts. However, the process of biopsy is destructive and small sample volume may lead to missed diagnosis [7]. Confocal Laser Endomicroscopy (CLE) can provide cellular/subcellular resolution to image the microstructures in GI tracts, but its limited field size may render it subject to sampling errors similar to those of endoscopic biopsy [8, 9].

Optical coherence tomography (OCT) is a promising three-dimensional imaging tool for obtaining real-time images for its non-invasive and high resolution properties [10, 11]. Fiber-optic endoscopic OCT techniques with spatial resolution of 7-30 μm have been developed for imaging gastrointestinal (GI) tracts [12-21]. Since it is straightforward to improve axial resolution of OCT by use of a light source with boarder spectral bandwidth, advances in ultrahigh axial resolution technique has significantly improved the image quality [22]. However, this lateral resolution is not enough to provide cellular-level information.

In order to improve both axial and lateral resolution of OCT devices, micro-optical coherence tomography (μOCT) with 1-3 μm spatial resolution has been developed to

visualize cellular and subcellular scale microstructures *ex vivo* [23-27] and a linear scanning flexible μOCT bronchoscope has been successfully demonstrated for imaging mucociliary clearance *in vivo* [28, 29]. However, no progress has been made to develop a circumferential scanning μOCT endomicroscope for GI tract imaging. The major technical difficulty is the well-known trade-off between the lateral resolution and depth of focus (DOF), which precludes practical applications of μOCT endomicroscopy.

In this paper, we propose a μOCT endomicroscopy system to mitigate the above-mentioned fundamental problem by use of a rigid sheath. We tested the capability of μOCT endomicroscope using fresh swine colon tissues, and the results verified the feasibility of circumferential scanning endomicroscopic μOCT for cellular-level resolution imaging.

2. Materials and Methods

2.1. μOCT imaging system

The endomicroscopic μOCT system consists of three parts: imaging console, rotary junction and fiber-optic probe (**Figure 1).** A supercontinuum light source (SC, Superk Extreme OCT, NKT Photonics, Birkerød Denmark) provides a broadband illumination over a spectral range of 650 nm - 1600 nm. The output was filtered by a short pass dichroic filter (DMSP1000; Thorlabs Inc., Newton, New Jersey, USA) to limit the source bandwidth at 650 nm – 1000 nm. We chose a 2x2 fiber coupler with a splitting ratio of 50:50 (Gould Fiber Optics, USA) to guide the output of the light source to the fiber-optic probe via a rotary junction. The illumination power delivered to the sample from the probe was measured to be 15.6 mW. The interference signal returning from the probe was collected by a spectrometer: the returning signal was collimated by a collimation lens L (AC127-030-B-ML, Thorlabs Inc., USA), dispersed by a diffraction grating G (960 lines/mm at 840 nm; Wasatch Photonics Inc. , Logan, Utah, USA), and then focused by a camera lens (Nikon AF Nikkor 85 mm f/1.8D, Tokyo,

Japan) onto a line scan CCD camera (E2V, AViiVA EM4-EV71YEM4CL2014-BA9). The detected spectrograms were finally transferred from the camera to a computer through camera link cables and an image acquisition card (KBN-PCECL4-F, Bitflow Inc., , Woburn, Massachusetts, USA) at 12-bit resolution. During the experiments, the camera was synchronized by a triggering signal of 20kHz generated by the computer, therefore, the system line scanning rate was 20k lines/s.

In the fiber-optic probe shown in **Figure 2(a)**, the light transmits through a single-mode fiber (SMF) (780HP, Thorlabs Inc., USA), which is protected by a glass ferrule (Accu-Glass LLC, St. Louis, Missouri, USA), to a BK7 glass spacer (1.8 mm Dia, GrinTech GmbH, Jena, Germany). To avoid back-reflection at the fiber-spacer interface, the ferrule and the spacer were angle-polished at 4 degrees. A gradient-index (GRIN) lens (GrinTech GmbH, Germany) with a diameter of 1.8 mm was used to focus the beam. A beamsplitter (BS) was cemented to the free end of the GRIN lens to divide the input light into a reference beam and a sample beam. To achieve common path between the reference and the sample arms, the beamsplitter is composed of two right angle prisms (Changchun Boxin Photoelectric Co., Changchun, China) with both hypotenuses cemented together a reflective annular metal coating in between. This beamsplitter design is similar to the previously report in [23, 28]: the wavefront of the optical beam was split into two portions with a center circular portion went directly through the beamsplitter towards the reference reflector (1 mm Dia, Prime Bioscience, Singapore), while the other annular portion reflected by 90 degree to the radial direction toward the sample. The backreflected reference beam and the backscatterred sample beam were recombined by the beamsplitter into the SMF along the same path. We used the ultraviolet cured optical adhesive (NOA 85, Edmund Optics Inc., Barrington, New Jersey, USA) to cement all optical components.

A Polyether ether ketone (PEEK) tube of 0.50 mm inner diameter and 1.59 mm outer diameter (Beijing Jianxin Technology Co., Beijing, China) was cemented to the ferrule as the

driveshaft (**Figure 2(b) and (c)**). A transparent glass tube (1.818 mm inner diameter and 2.8 mm outer diameter, Thorlabs Inc., USA) was used in place of the commonly used polymer sheath to maintain a circular lumen and center the distal end optics with regard to the tissue lumen (Figure 2(c)). The glass tube was immobilized by a thin heat shrink tube which was connected to the metal housing of the probe (Figure 2(c)). During the circumferential scanning, both the outer housing and the transparent glass tube were immobilized to translation stages (HFF001, APY001/M and MBT616D, Thorlabs Inc., USA) while the inner probe was rotated. The rotary joint comprises of a motorized rotation stage (Newport, Irvine, California, USA), a fiber rotary joint (Princetel Inc., Hamilton Township, New Jersey, USA), and a customized timing belt pulley to transmit the rotation motion from the motorized stage to the probe.

2.2 System characterization

The axial resolution of the system was measured by detecting the full width at half-maximum (FWHM) of the axial point spread function (PSF) with a glass reflector as the sample. We used a tilted glass reflector (with an attenuation of 33.7 dB) in the focal plane of the sample arm to characterize the axial resolution and sensitivity.

To testify the transverse resolution, we utilized a laser beam profiler (LBP2-HR-VIS2, Newport, USA) together with an objective (50× DRY Plan Fluorite Objective, Nikon, Japan) to capture the in-focus sample beam. DOF represents the axial distance over which the beam size at the 1/e2 beam is not larger than two times of that at the beam waist, and it also can be measured by the laser beam profiler. To further confirm the transverse resolution and DOF measured by above-mentioned method, we conducted imaging experiments to measure the FWHM of the transverse profile with a home-made microparticles phantom as the sample consisting of the micro-beads (the standard size of 2 μm, Polyscience Inc., Warrington,

Pennsylvania, USA) mixed with the agarose solution (No. PC0701-100g, Vivantis Inc. , Oceanside, California, USA).

2.3 Imaging protocol and swine imaging

To validate the capability of endomicroscopic imaging, *ex vivo* imaging experiments with this probe-based endomicroscopic μOCT system were conducted on freshly explanted swine colon tissues. We collected the swine colon tissues for endomicroscopic μOCT imaging from a slaughterhouse in Singapore. We opened up the tissue lumen and dissected the tissues into rectangular shape of 7.0 mm by 10.0 mm before attaching each tissue to the outer surface of the glass tube. During circumferential scanning, the imaging rate was 1 revolution/sec which was limited by the speed of the motorized rotation stage. When finishing the experiments, we marked the region of interests (ROIs) using tissue marking dye and then fixed the tissues using 4% neutral buffered formaldehyde for histological analysis in comparison with μOCT images. We performed 2-frame averaging (time-lapse averaging) and software based speckle reduction [30, 31] to reduce the speckle of the images and enhance the cellular-level structural contrast.

3. Results and Discussion

The result in **Figure 3(a)** indicates that the axial resolution was 2.48 μm in air, and the corresponding resolution in tissue is 1.81 μm in tissue (assuming the refractive index n=1.37). The measured SNR of the -33.7 dB reflector was 65.1 dB (**Figure 3(b)**), so that the sensitivity of this system was tested to be 98.8 dB.

The transverse resolution was designed to be 3.6 μm. Indicated in the **Figure 3(c)**, the spot size of the beam at the focal plane (Depth = 210 μm) was measured to be 4.8 μm by the laser beam profiler, which is also confirmed by the transverse profile of a microparticle (**Figure 3(d)**). The irregular intensity distribution of the measured PSFs in Figures 3(c) was caused by

fabrication defects in the annular metal coating of the beamsplitter. Besides, the DOF of the fabricated probe was measured to be ~150 μm.

The path length difference between the reference and the sample focus was maintained to be 215.3 μm. The distance between the sample surface and the center of the probe was about 1.516 mm so that the focus was 116 μm away from the outer surface of the glass tube.

In representative cross-sectional images of swine colon mucosa (**Figure 4 and Figure 5),** in addition to the layered structures of the mucosa, the crypt profiles including crypt lumens (white arrows, **Figure 4(b), (c), (d) and Figure 5(b), (c), (d)**) can also be clearly visualized. Owning to the improved spatial resolution, we are able to pick up cellular-level microstructures, such as the mucus-laden goblet cells (yellow arrow heads, Figure 4(b), (c), (d) and Figure 5(b), (c), (d)), which are consistent with the previously published results using a desktop μOCT system [32]. More importantly, when comparing the endomicroscopic μOCT images with corresponding histology image (**Figure 4(e)**), a good correlation between μOCT images and the histology can be clearly observed, convincingly confirming the above-mentioned findings.

The improved spatial resolution achieved by the proposed endomicroscope enables visualization of cellular-level structures in GI tracts, which has never been reported to the best of our knowledge. The results underscore the critical role of high lateral resolution in visualizing cellular-level details in comparison with those obtained with lower lateral resolution systems [22]. According to the previous results obtained using a desktop μOCT system [32], the ideal lateral resolution is ~2 μm or below. The current lateral resolution of 4.8 μm is still not enough for resolving more cellular-level details, such as columnar epithelial cells.

The common-path probe with apodization design adopted can extend DOF moderately while maintain the high transverse resolution [23, 28]. Further improvement in lateral resolution requires DOF extension techniques such as phase modulation for producing quasi-

Bessel beams through a cylindrical waveguide or a phase mask [33, 34]. Our further study will focus on endoscopic μOCT probe with higher extended DOF without the compromise of high resolution for clinical application.

We employed a rigid glass tube to mitigate the issue of limited DOF so that crypts structures were properly maintained around the relative small focal region. However, this glass tube may not be a viable option for clinical applications. Moving forward, this glass tube can be replaced by a polymer capsule, similar to the previously reported tethered capsule design [17]. The outer diameter of the capsule can be tailored according to the GI tract to be imaged. For smaller lumens such as pancreatic and bile ducts, a diameter of 1.5 - 2 mm might be suitable.

The corresponding histology image (Hematoxylin & eosin) does not show any significant tissue structural damage due to mechanical stress of the probe scanning (Figure 4(e)). This is because that the optical probe was scanning inside the stationary transparent glass tube, which isolated the tissue from the mechanical stress induced by the mechanical scanning of the distal end optics. In addition, the light power on the tissue was 15.6 mW, which was smaller than the power used in previous studies in which no tissue alterations due to light interactions with tissue were reported. For example, Cui et al reported a sample power of 18 mW in the same wavelength range as the current study [29].

The inner surface of the transparent glass tube covering the probe would present strong back-reflection when the sample light goes through the air-glass interface. To alleviate its influences, we applied water to fill the space (air) between the beamsplitter and the inner surface of the transparent tube during the experiments. Even though the back-reflection of the inner surface of the tube was mitigated, it is still highly stronger than the reflection by the scattered tissues (swine colon in this study). Hence, the conjugated profile of the inner surface of the transparent tube is still clearly displaced in **Figure 4(a) and Figure 5(a)**. Our next-step

work is to remove or reduce it to a sustainable level to minimize influences on the imaging results, and a possible solution could be to slightly adjust the angle between the sample beam and the inner surface of the tube.

We also found that the contrast of cellular-level details is very sensitive to speckle noise as shown in **Figure 6**. Of course, inter-frame averaging will be very difficult to realize simplely due to the motion artifacts caused by the sample and probe motion. To solve this issue, multifiber angular compounding OCT [35] may be a candidate choice in the future, since it is able to achieve inter-A-line averaging, which is significantly less sensitive to motion artifacts.

The proposed high resolution of endomicroscopic μOCT can capture more subtle morphological features and would be beneficial to diagnose cancers at an early stage, and thus could pave the way for the surveillance, detection and treatment of GI tracts diseases.

5. Conclusion

In summary, we designed and fabricated a flexible endomicroscopic μOCT probe with cellular resolution for visualization swine colon *ex vivo*. The cellular-level microstructures such as the intestinal crypts and goblet cells can be clearly resolved, demonstrating that this probe-based μOCT system is capable of imaging the cellular-level morphology and thus provides the probability of evaluating the pathological lesions of GI cancers at an early stage. Furthermore, the flexibility of this probe renders it traverse through the inner lumen of the tissue for circumferential visualizing. Additionally, the usage of the rigid glass tube can mitigate the issue of limited DOF so that crypts structures were properly maintained around the relative small focal region. And in the future, a polymer capsule would be employed to replace the glass tube for clinical applications.

Acknowledgements We sincerely appreciate funding support from National Research Foundation Singapore (NRF-CRP13-2014-05), Ministry of Education Singapore (MOE2013-

T2-2-107), National Medical Research Council Singapore (NMRC/CBRG/0036 /2013) and NTU-AIT-MUV program in advanced biomedical imaging (NAM/15005).

References

[1] H. Clevers, *Cell* **154**, 274-284 (2013).

[2] J.R. McDole, L.W. Wheeler, K.G. McDonald, B. Wang, V. Konjufca, K.A. Knoop, R.D. Newberry and M.J. Miller, *Nature* **483**, 345-349 (2012).

[3] T. Pelaseyed, J.H. Bergström, J.K. Gustafsson, A. Ermund, G.M. Birchenough, A. Schütte, S. Post, F. Svensson, A.M. Rodríguez‐Piñeiro and E.E. Nyström, *Immunol. Rev.* **260**, 8-20 (2014).

[4] P. Correa, M.B. Piazuelo and K.T. Wilson, *Am. J. Gastroenterol.* **105**, 493 (2010).

[5] A.-M. Baker, B. Cereser, S. Melton, A.G. Fletcher, M. Rodriguez-Justo, P.J. Tadrous, A. Humphries, G. Elia, S.A. McDonald and N.A. Wright, *Cell Rep.* **8**, 940-947 (2014).

[6] A. Humphries and N.A. Wright, *Nat. Rev. Cancer* **8**, 415-424 (2008).

[7] P. Sharma, R.H. Hawes, A. Bansal, N. Gupta, W. Curvers, A. Rastogi, M. Singh, M. Hall, S.C. Mathur and S.B. Wani, *Gut* **62**, 15-21 (2013).

[8] G.W. Falk, T.W. Rice, J.R. Goldblum and J.E. Richter, *Gastrointest. Endosc.* **49**, 170-176 (1999).

[9] R. Kiesslich, M. Goetz, M. Vieth, P.R. Galle and M.F. Neurath, *Nat. Clin. Pract. Oncol.* **4**, 480-490 (2007).

[10] D. Huang, E.A. Swanson, C.P. Lin, J.S. Schuman, W.G. Stinson, W. Chang, M.R. Hee, T. Flotte, K. Gregory and C.A. Puliafito, *Science* **254**, 1178 (1991).

[11] G.J. Tearney, M.E. Brezinski, B.E. Bouma, S.A. Boppart, C. Pitris, J.F. Southern and J.G. Fujimoto, *Science* **276**, 2037-2039 (1997).

[12] M.V. Sivak, K. Kobayashi, J.A. Izatt, A.M. Rollins, R. Ung-Runyawee, A. Chak, R.C. Wong, G.A. Isenberg and J. Willis, *Gastrointest. Endosc.* **51**, 474-479 (2000).

[13] D.C. Adler, Y. Chen, R. Huber, J. Schmitt, J. Connolly and J.G. Fujimoto, *Nat. Photonics* **1**, 709-716 (2007).

[14] S.H. Yun, G.J. Tearney, B.J. Vakoc, M. Shishkov, W.Y. Oh, A.E. Desjardins, M.J. Suter, R.C. Chan, J.A. Evans and I.-K. Jang, *Nat. Med.* **12**, 1429-1433 (2006).

[15] E. Zagaynova, N. Gladkova, N. Shakhova, G. Gelikonov and V. Gelikonov, *J. Biophotonics* **1**, 114-128 (2008).

[16] M.J. Suter, B.J. Vakoc, P.S. Yachimski, M. Shishkov, G.Y. Lauwers, M. Mino-Kenudson, B.E. Bouma, N.S. Nishioka and G.J. Tearney, *Gastrointest. Endosc.* **68**, 745-753 (2008).

[17] M.J. Gora, J.S. Sauk, R.W. Carruth, K.A. Gallagher, M.J. Suter, N.S. Nishioka, L.E. Kava, M. Rosenberg, B.E. Bouma and G.J. Tearney, *Nat. Med.* **19**, 238-240 (2013).

[18] T.-H. Tsai, O.O. Ahsen, H.-C. Lee, K. Liang, M. Figueiredo, Y.K. Tao, M.G. Giacomelli, B.M. Potsaid, V. Jayaraman and Q. Huang, *Gastroenterology* **147**, 1219 (2014).

[19] W. Yuan, J. Mavadia-Shukla, J. Xi, W. Liang, X. Yu, S. Yu and X. Li, *Opt. Lett.* **41**, 250-253 (2016).

[20] H.-C. Lee, O.O. Ahsen, K. Liang, Z. Wang, C. Cleveland, L. Booth, B. Potsaid, V. Jayaraman, A.E. Cable and H. Mashimo, *Biomed. Opt. Express* **7**, 2927-2942 (2016).

[21] W.A. Welge and J.K. Barton, *Lasers in surgery and medicine* **49**, 249-257 (2017).

[22] A.R. Tumlinson, J.K. Barton, B. Považay, H. Sattman, A. Unterhuber, R.A. Leitgeb and W. Drexler, *Opt. Express* **14**, 1878-1887 (2006).

[23] L. Liu, J.A. Gardecki, S.K. Nadkarni, J.D. Toussaint, Y. Yagi, B.E. Bouma and G.J. Tearney, *Nat. Med.* **17**, 1010-1014 (2011).

[24] L. Liu, K.K. Chu, G.H. Houser, B.J. Diephuis, Y. Li, E.J. Wilsterman, S. Shastry, G. Dierksen, S.E. Birket and M. Mazur, *PloS one* **8**, e54473 (2013).

[25] K.K. Chu, G.J. Ughi, L. Liu and G.J. Tearney, *Curr. Cardiovasc. Imaging Rep.* **7**, 1-8 (2014).

[26] D. Cui, X. Liu, J. Zhang, X. Yu, S. Ding, Y. Luo, J. Gu, P. Shum and L. Liu, *Opt. Lett.* **39**, 6727-6730 (2014).

[27] X. Yu, X. Liu, S. Chen, Y. Luo, X. Wang and L. Liu, *Opt. Express* **23**, 26399-26413 (2015).

[28] K.K. Chu, C. Unglert, T.N. Ford, D. Cui, R.W. Carruth, K. Singh, L. Liu, S.E. Birket, G.M. Solomon and S.M. Rowe, *Biomed. Opt. Express* **7**, 2494-2505 (2016).

[29] D. Cui, K.K. Chu, B. Yin, T.N. Ford, C. Hyun, H.M. Leung, J.A. Gardecki, G.M. Solomon, S.E. Birket and L. Liu, *Opt. Lett.* **42**, 867-870 (2017).

[30] I.W. Selesnick, *IEEE Trans. Sig. Process.* **52**, 1304-1314 (2004).

[31] A. Zhang, J. Xi, J. Sun and X. Li, *Biomed. Opt. Express* **8**, 1721-1730 (2017).

[32] X. Yu, Y. Luo, X. Liu, S. Chen, X. Wang, S. Chen and L. Liu, *IEEE Photonics J.* **8**, 1-8 (2016).

[33] B. Yin, K.K. Chu, C.-P. Liang, K. Singh, R. Reddy and G.J. Tearney, *Opt. Express* **24**, 5555-5564 (2016).

[34] J. Kim, J. Xing, H.S. Nam, J.W. Song, J.W. Kim and H. Yoo, *Opt. Lett.* **42**, 379-382 (2017).

[35] D. Cui, E. Bo, Y. Luo, X. Liu, X. Wang, S. Chen, X. Yu, S. Chen, P. Shum and L. Liu, *Opt. Lett.* **42**, 125-128 (2017).

Figure 1. Schematic of the endomicroscopic μOCT system with the fiber-optic probe. SCL：Supercontinuum light source. FC: fiber coupler; L: achromatic lens; G: grating; CCD: charge-coupled device; PC: personal computer.

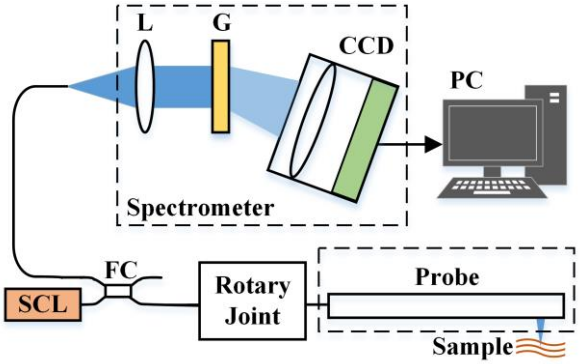

Figure 2. Illustration of the endomicroscopic μOCT probe. (a) Schematic diagram of the fiber-optic probe. 1: driveshaft; 2: single mode fiber; 3: ferrule; 4: glass spacer; 5: GRIN lens; 6: beamsplitter; 7: reference reflector. (b) Photograph of the fiber-optic probe with the brown Polyether ether ketone (PEEK) tube as the driveshaft. (c) Photograph of the fiber-optic probe connected to a rotary joint. FRJ: fiber rotary joint; MRS: motorized rotation stage; TBP: timing belt pulley. TS: translation stages.

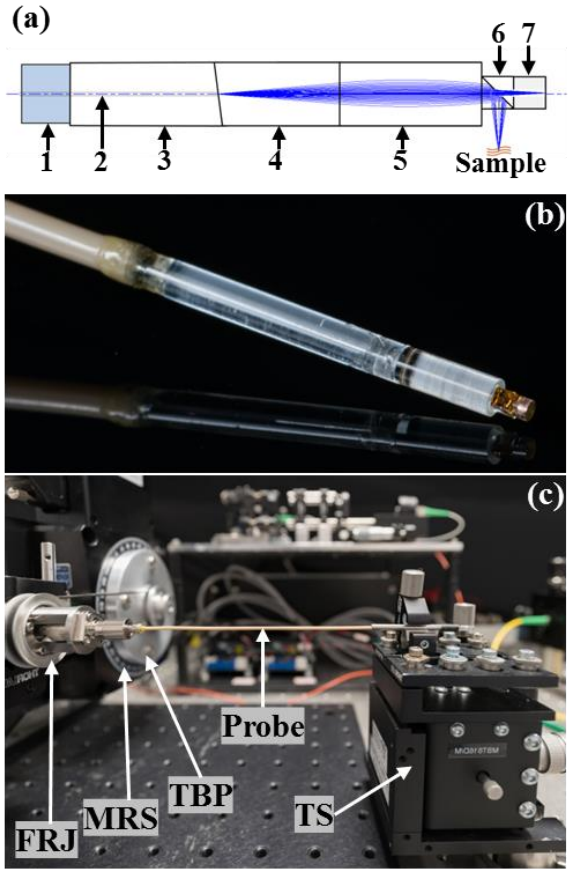

Figure 3. Characterization of the endomicroscopic µOCT system. (a) Measured axial profile of the constructed endomicroscopic µOCT system by using a glass reflector as the sample. (b) Measured axial profile acquired with a glass reflector (red curve) vs. measured noise floor with reference light only (blue curve). The noise floor was averaged over 256 A-lines. The signal power was plotted in a log scale. (c) Two-dimension images of the beam profile at three different axial depths. Transverse profiles and lateral profiles were displayed in bottom and left sides, respectively. Intensity is scaled in color bar. (d) µOCT image of the microparticles phantom (upper left) and measured transverse profiles at three different axial depths obtained from the µOCT image.

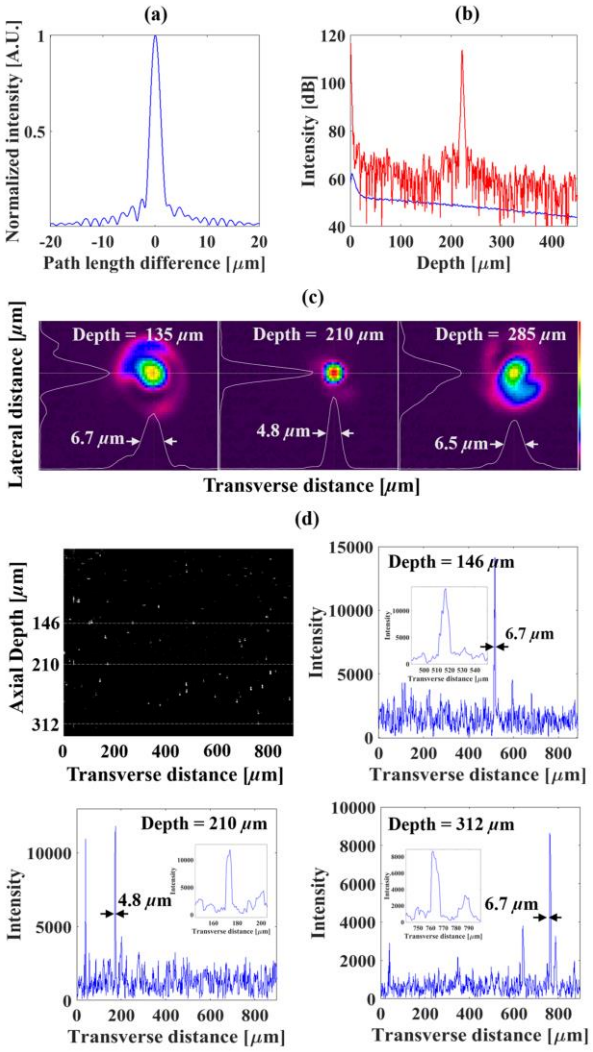

Figure 4. Cross-sectional images of a normal swine colon *ex vivo*. (a) Representative cross-sectional µOCT image during circumferential scanning: it consists of 900 pixels (axial, 893.7 µm) × 6200 pixels (circumferential, minimum circle: 8375.5 µm). Red arrow indicates the conjugated profile of the inner surface of the transparent tube covering the probe. The cellular structures such as crypt lumens and goblet cells can be obviously captured in the indicated areas by red boxes. (b-d) Respective zoomed-in views of three red boxes in (a) showing crypt lumens (white arrows) and goblet cells (yellow arrow heads). Image Size: 475.5 µm (circumferential, minimum circle) × 484.6 µm (axial). (e) Representative histology, hematoxylin and eosin (H&E) staining. Black arrows indicate crypt lumens, and the yellow arrow heads indicate goblet cells. Scale bars: 100 µm.

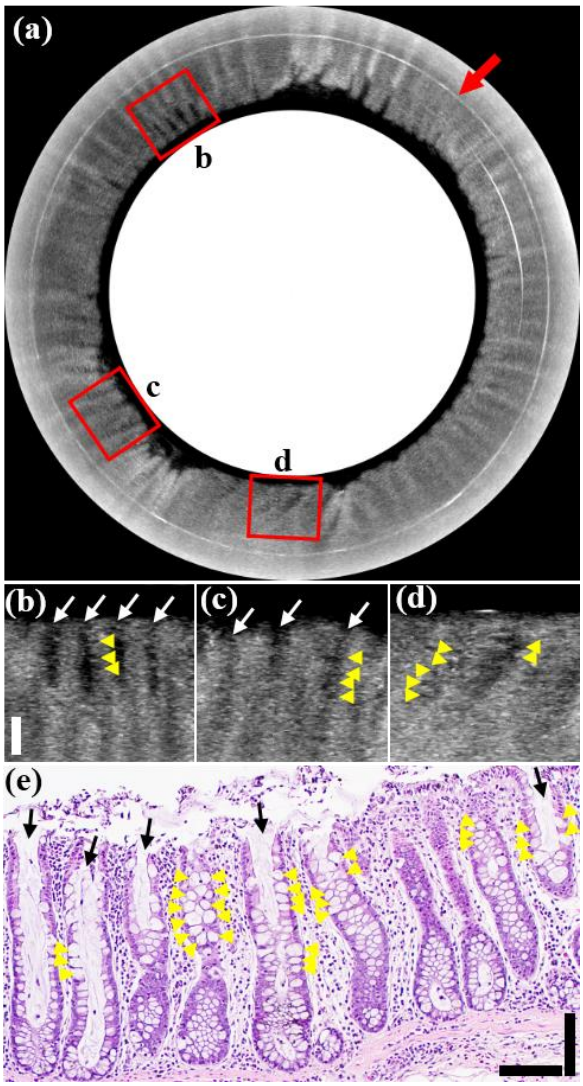
(a)
b
c
d
(b)
(c)
(d)
(e)

Figure 5. Cross-sectional images of a normal swine colon *ex vivo* by endomicroscopy µOCT system. (a) Representative cross-sectional µOCT image during circumferential scanning: it consists of 900 pixels (axial, 893.7 µm) × 6200 pixels (circumferential, minimum circle: 8375.5 µm). Red arrow indicates the conjugated profile of the inner surface of the transparent tube covering the probe. The cellular structures such as crypt lumens and goblet cells can be obviously captured in the indicated areas by red boxes. (b-d) Respective zoomed-in views of three red boxes in (a) showing crypt lumens (white arrows) and goblet cells (yellow arrow heads). Image Size: 475.5 µm (circumferential, minimum circle) × 484.6 µm (axial). Scale bar: 100 µm.

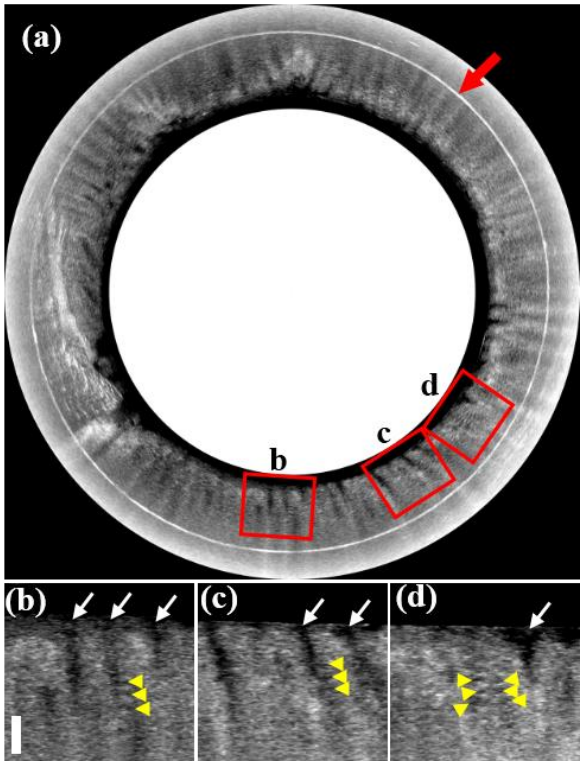

Figure 6. Comparison of µOCT images with and without frame averaging and speckle reduction algorithm. (a-c) µOCT images with frame averaging and speckle reduction algorithm. (a'-c') Original µOCT images without frame average and speckle reduction algorithm corresponding to (a-c). Scale bar: 100 µm.

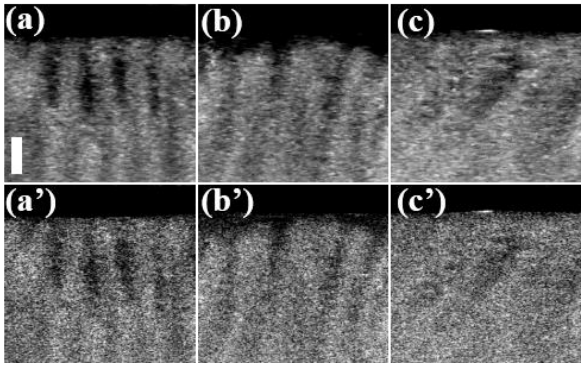

Gaphical Abstract

This paper presents a μOCT endomicroscopy system capable of acquiring cellular level details of gastrointestinal tissues through circumferential scanning with 2.48-μm axial resolution and 4.8-μm transverse resolution along the DOF of ~150 μm. The imaging results demonstrate the feasibility of this fiber-optic μOCT system for visualizing cellular-level morphological features, which paves the way for the surveillance, detection and treatment of gastrointestinal tracts diseases.